

# Aggregation Kinetics of Multiwalled Carbon Nanotubes in Aquatic Systems: Measurements and Environmental Implications

NAVID B. SALEH, LISA D. PFEFFERLE,  
AND MENACHEM ELIMELECH\*

Department of Chemical Engineering, Yale University,  
New Haven, Connecticut 06520-8286

Received May 7, 2008. Revised manuscript received August 6, 2008. Accepted August 11, 2008.

The initial aggregation kinetics of multiwalled carbon nanotubes (MWNTs) were examined through time-resolved dynamic light scattering. Aggregation of MWNTs was evaluated by varying solution pH and the concentration of monovalent (NaCl) and divalent (CaCl<sub>2</sub> and MgCl<sub>2</sub>) salts. Suwannee River humic acid (SRHA) was used to study the effect of background natural organic matter on MWNT aggregation kinetics. Increasing salt concentration and addition of divalent calcium and magnesium ions induced MWNT aggregation by suppressing electrostatic repulsion, similar to observations with aquatic colloidal particles. The critical coagulation concentration (CCC) values for MWNTs were estimated as 25 mM NaCl, 2.6 mM CaCl<sub>2</sub>, and 1.5 mM MgCl<sub>2</sub>. An increase in solution pH from acidic (pH 3) to basic (pH 11) conditions resulted in a substantial (over 2 orders of magnitude) decrease in MWNT aggregation kinetics, suggesting the presence of ionizable functional groups on the MWNT carbon scaffold. The presence of humic acid in solution markedly enhanced the colloidal stability of MWNTs, reducing the aggregation rate by nearly 2 orders of magnitude. The enhanced MWNT stability in the presence of humic acid is attributable to steric repulsion imparted by adsorbed humic acid macromolecules. Our results suggest that MWNTs are relatively stable at solution pH and electrolyte conditions typical of aquatic environments.

## Introduction

Carbon nanotubes (CNTs) are allotropes of carbon with exceptional physicochemical, optical, and mechanical properties (1, 2). Rolled-up graphene sheets of carbon nanotubes having cage-like architecture similar to the geodesic dome-shaped buckyballs, can be single-shelled (3) or multiple-concentric shelled (4), termed, respectively, single-walled (SWNT) and multiwalled (MWNT) carbon nanotubes. SWNTs, MWNTs, and their derivatives and hybrids have a wide variety of applications, including microelectronics (5), energy storage (6), composite construction materials (7), nanopropes and sensors (8), and vehicles for drug delivery (9). These helical microtubules with their extraordinary properties are emerging as a new class of nanomaterials in electronic, pharmaceutical, and energy industries.

Extensive use of CNTs in industry and the consumer market has increased the likelihood of CNT exposure to the

natural environment. CNTs can be released into the environment via wastewater discharge and point source emissions from manufacturing industries (10). Upon release, nanomaterials are likely to interact with aquatic surfaces and biological species as well as aggregate, depending on the interplay between electrostatic and van der Waals interactions (11). The aggregation state of CNTs has a strong influence on their fate and transport in the environment. Understanding the factors governing the aggregation behavior of CNTs is a key to evaluating their environmental transport, fate, and potential interaction with biological species.

To date, the only study reporting the aggregation behavior of CNTs is that by Sano et al. (12) where the state of aggregation of acid-treated SWNTs was monitored by UV absorbance in solutions containing several inorganic salts. The current literature on CNT aggregation mostly involves the enhancement of their aqueous solubility, either by dispersing CNTs by surfactant (13, 14) or polymer adsorption (15), or by incorporating functional groups through acid treatment (1, 16). There are only a handful of publications that study CNT aggregate structure. Chen et al. (17) studied CNT aggregate structure in water through light scattering and predicted the fractal dimension of surfactant-modified and acid-treated SWNTs. Niyogi et al. (18) studied differences in spectroscopic signatures of SWNTs at different NaCl concentrations to infer about the SWNT aggregation state. Yet, the aggregation kinetics of CNTs in aqueous systems have not been examined in previous studies. In particular, there is a critical need to understand and quantify the influence of solution chemistry and the presence of natural organic matter on the rate of CNT aggregation.

The objective of this paper is to investigate the early stage aggregation kinetics of MWNTs under various environmentally relevant solution chemistries. These include variations in monovalent (NaCl) and divalent (CaCl<sub>2</sub> and MgCl<sub>2</sub>) salt concentrations, solution pH, and the presence of natural organic matter (Suwannee River humic acid). MWNT stability curves, i.e., the logarithm of the MWNT attachment efficiency versus the logarithm of salt concentration, are constructed using the aggregation kinetics data, from which the critical coagulation concentrations for the various salts are determined. The measured electrokinetic and other physicochemical properties of MWNTs are used to elucidate the aggregation mechanisms.

## Materials and Methods

**Preparation of MWNTs.** We used commercially available MWNTs (composite grade, lot no. JS02230701, NanoTechLabs Inc., Yadkinville, NC). The manufacturer reports that the sample is over 95% by mass MWNT, with a powder density of 2.1 g/cm<sup>3</sup> at 20 °C. It is also reported that the MWNTs are on average 20–40 nm in diameter and 50 μm in length. MWNT purity and size distributions are independently determined in this study.

The MWNT samples for aggregation experiments were prepared using a successive sonication and clarification protocol (19). First, 50 mg of as-received (untreated) MWNT powder was added to 500 mL deionized water (Barnstead). The mixture was then sonicated continuously using an ultrasonication probe (Misonix 3000, Misonix Inc., Farmingdale, NY) for 30 min at 4.5 dial strength. The MWNT suspension was left aside quiescently at room temperature for 10 min and the stable supernatant was collected. The collected supernatant was sonicated following the same procedure for five additional cycles and each time only the stable suspension was collected. The final collected

\* Corresponding author phone: (203) 432-2789; e-mail: menachem.elimelech@yale.edu.

MWNT stock was stable for the duration of all the aggregation experiments.

**Characterization of MWNTs.** MWNT samples were characterized for size distribution, purity, and key physicochemical properties for both the as received (untreated) and the sonicated (treated) samples. The electrophoretic mobility (EPM) measurements and imaging of tubes were done with samples from the same stock used for aggregation experiments. Raman spectroscopy and thermogravimetric analysis (TGA) require higher mass of samples. To obtain significant mass to perform these measurements, a new stock was prepared using six cycles of successive sonication, but the entire mass of MWNTs was retained throughout the six cycles of sonication.

The electrophoretic mobilities of MWNT samples were measured for a range of salt concentrations, pH, and in the presence of Suwannee River humic acid (SRHA) with the ZetaPALS analyzer (Brookhaven Instrument Corp., Holtsville, NY) at 24 °C. MWNT suspension was diluted by a factor of 10 from the aggregation stock for the EPM measurements. Salt solutions, acid/base, and SRHA were added immediately prior to the EPM measurements to mimic the aggregation experiments. At least 30–40 measurements were done for each solution condition.

A high resolution transmission electron microscope (Tecnai G2, FEI Company, Eindhoven, Netherlands) was used to image MWNT samples before and after treatment. The as-received MWNT sample was dispersed in ethanol (for better debundling) and treated MWNT sample in aqueous solution was used from the stock for aggregation experiments. A drop of the MWNT suspension was placed directly on a nickel TEM grid coated with carbon-Formvar and left to adsorb for 2 min. The excess water was then absorbed with a filter paper. For determining the diameter and length distribution data of untreated and treated MWNT samples, at least 100 images were taken for each case. Nanotube diameter and length were measured using the iTEM software (Olympus Soft Imaging Solutions, Münster, Germany).

Raman spectra were recorded with untreated and treated MWNTs using a Jasco multiwavelength NRS-3000 series Raman spectrometer (Jasco Inc., Easton, MD) equipped with a confocal microscope, anastigmatic 300 mm focal length spectrograph, and a thermoelectrically cooled charged coupled device (CCD). Integration time was 15 s for each spectrum, with each spectrum representing the average of five scans. The spectra were obtained at two different wavelengths: 785 nm (1.58 eV) and 532 nm (2.33 eV).

Purity of the untreated and treated MWNT samples was determined from thermogravimetric analysis (TGA) (SetSys 1750, Setaram Instrumentation, Caluire, France) using a holey crucible. An as-received MWNT sample of 18.87 g was used for TGA, where the sample was heated at a constant temperature ramp of 10 °C/min up to 1000 °C in the presence of oxygen. The weight loss of the sample was monitored throughout the heating process.

**Solution Chemistry.** MWNT aggregation experiments were conducted with monovalent (NaCl) and divalent (CaCl<sub>2</sub> and MgCl<sub>2</sub>) electrolyte solutions (reagent grade, J. T. Baker, Phillipsburg, NJ) over a wide concentration range. The pH of the MWNT suspensions at all salt concentrations was unadjusted (ambient) and measured at 6.0 ± 0.2. For the specific runs with MWNT samples at pH 3 and 11, freshly prepared 0.1 M HCl and NaOH solutions were used, respectively, to adjust the pH. All reagent solutions were filtered with 0.1 μm (Anotop 25, Whatman, Middlesex, UK) inorganic membrane filters.

**Humic Acid Solution.** Suwannee River humic acid, SRHA (Standard II, International Humic Substances Society), was used as a model natural organic matter. The humic acid stock solution was prepared by introducing 20.5 mg of the

dry humic acid powder to 50 mL filtered deionized water and stirring the solution overnight in the dark. The solution was then filtered under vacuum using a 0.22 μm cellulose acetate membrane filter (Corning Inc., Corning, NY). The pH of the stock SRHA was raised from 3.2 to 6.0 by adding NaOH, and the stock was subsequently stored in the dark at 4 °C. The total organic carbon content of the SRHA stock solution was found to be 2.54 mg/L TOC through high temperature oxidation (TOC-VCHS, Shimadzu, Kyoto, Japan). This concentration of SRHA is typical of natural surface waters (20). The key properties of the SRHA are given elsewhere (21, 22).

**MWNT Aggregation.** The aggregation experiments were performed using a multiangle light scattering unit (ALV-5000, Langen, Germany) equipped with a solid-state Nd:vanadate (Nd:YVO<sub>4</sub>) laser (Verdi V2, Coherent, Santa Clara, CA) providing a single-frequency output of 532 nm. Further details of the instrument are described elsewhere (23). The MWNT samples were placed in new glass vials (Supelco, Bellefonte, PA) that were previously soaked in a cleaning solution (Extran MA 01, Merck KGaA, Darmstadt, Germany) overnight, thoroughly rinsed in deionized water, and oven-dried under dust-free conditions. The MWNT samples used in the aggregation experiments were diluted by a factor of 3 from the original stock. Electrolyte solutions, pH adjusting reagents, and/or SRHA were added prior to the aggregation experiments following the protocol described by Chen and Elimelech (21, 24). The dynamic light scattering measurements were conducted by positioning the detector at 90° with the incident laser beam and the autocorrelation function having been allowed to accumulate for over 15 s. The measurements were performed for a time period ranging from 20 min to 3 h to obtain an approximately 30% increase in the original hydrodynamic radius of MWNTs.

The initial aggregation rate constant of MWNTs is proportional to the initial rate of increase in the hydrodynamic radius,  $R_h$ , with time,  $t$ , and the inverse of MWNT concentration  $N_0$  (21):

$$k \propto \frac{1}{N_0} \left( \frac{dR_h(t)}{dt} \right)_{t \rightarrow 0}$$

Because the MWNT concentration in all aggregation experiments was identical, the attachment efficiency,  $\alpha$ , is readily obtained by normalizing the initial slope of the aggregation profile of a given solution chemistry by the initial slope obtained for favorable (fast) aggregation conditions:

$$\alpha = \frac{\frac{1}{N_0} \left( \frac{dR_h(t)}{dt} \right)_{t \rightarrow 0}}{\frac{1}{N_{0,\text{fav}}} \left( \frac{dR_h(t)}{dt} \right)_{t \rightarrow 0,\text{fav}}} = \frac{\left( \frac{dR_h(t)}{dt} \right)_{t \rightarrow 0}}{\left( \frac{dR_h(t)}{dt} \right)_{t \rightarrow 0,\text{fav}}}$$

where the subscript “fav” represents favorable solution conditions, where fast, diffusion-limited aggregation takes place. Note that the attachment efficiency,  $\alpha$ , is the inverse of the Fuchs stability ratio,  $W$ , commonly used in colloidal stability studies.

## Results and Discussion

**MWNT Electrokinetic Properties.** The electrokinetic properties of treated MWNTs in the form of electrophoretic mobility (EPM) as a function of salt concentration and pH are presented in Figure 1. Experimental measurements show that carbon nanotubes exhibit negative surface potential in aqueous systems, consistent with previously reported studies (12, 13). Increasing the monovalent and divalent salt concentration made the EPM values of the MWNTs less negative, as is commonly observed with most colloidal particles in aqueous solutions. There was a clear effect of pH on electrokinetic properties of MWNTs. As pH was increased from acidic to basic conditions (from 3 to 11), the EPM of

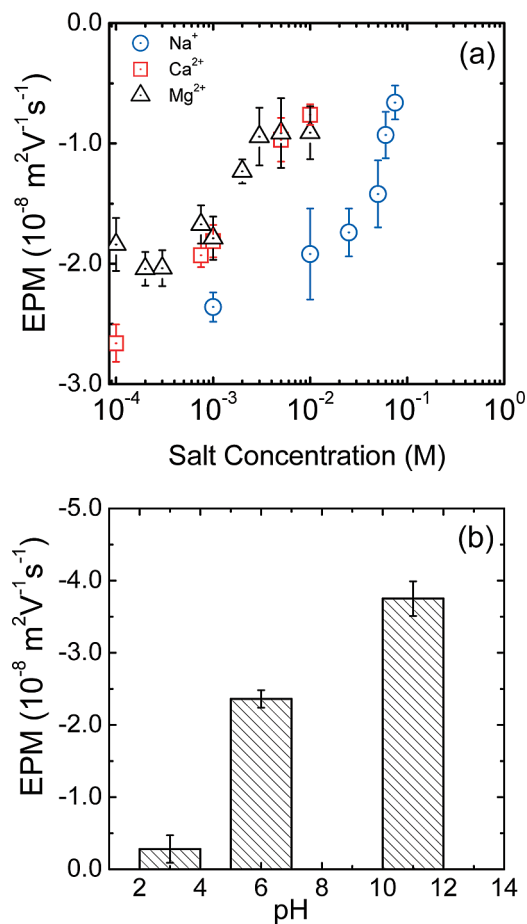


**FIGURE 1.** Electrophoretic mobility (EPM) of MWNTs as a function of (a) monovalent and divalent salts ( $\text{NaCl}$ ,  $\text{CaCl}_2$ , and  $\text{MgCl}_2$ ) and (b) solution pH. For EPM as a function of salt concentration, the pH was unadjusted ( $\text{pH } 6.0 \pm 0.2$ ). Measurements of EPM as a function of pH were carried out with 1 mM  $\text{NaCl}$  as a background electrolyte. Temperature for all EPM measurements was maintained at 24 °C.

MWNTs became more negative (from  $-(0.28 \pm 0.2) \times 10^{-8}$  to  $-(3.75 \pm 0.2) \times 10^{-8} \text{ m}^2 \text{ V}^{-1} \text{ s}^{-1}$ ). The marked increase in surface potential due to increases in solution pH indicates the presence of ionizable functional groups on MWNT surfaces. At this writing, the origin of surface charge is not fully understood for unfunctionalized carbon-based nanomaterials such as fullerenes and CNTs. Self-consistent mathematical models based on Fermi theory were used in a number of studies to describe the electron density distribution of fullerenes (25) and CNTs (26). The outer surfaces of the fullerenes and CNTs are shown to have high electron density, and can be taken as a possible explanation for the negative surface potential of these carbon-only materials. However, unlike fullerene nanoparticles (like  $n\text{C}_{60}$ ), CNTs have defects in the form of pentagon and heptagon irregularities at their carbon scaffold and also incomplete carbon rings at the end termini (27). These irregular sites on the sidewalls and tube-ends are susceptible to oxidation and the formation of carboxyl and hydroxyl functional groups (27). The presence of such functional groups explains the strong dependence of EPM on solution pH. Note that our sonication treatment can enhance the defects on MWNTs as will be discussed later when analyzing the Raman spectra.

Figure S1 in the Supporting Information (SI) presents the EPM of MWNTs in the presence and absence of SRHA. SRHA had a negligible effect on the MWNT EPM under the solution chemistries investigated. The slight reduction in EPM in the presence of divalent cations is likely attributed to specific

interactions of  $\text{Ca}^{2+}$  and  $\text{Mg}^{2+}$  with the  $-\text{COOH}$  functional groups in SRHA as observed elsewhere (21, 28).

**MWNT Size and Shape.** TEM imaging before sonication (Figure 2a) shows that the as-received MWNTs are long and heavily bundled. Most of the MWNTs appeared to have thick external walls, indicating the presence of multiple concentric walls. The dark spherical features on the image are most likely catalyst particles. These catalyst particles are occasionally present inside the nanotube structure as well as terminal features (29). Figure 2b shows significant debundling and shortening of length of the MWNTs after sonication. Isolated single MWNTs were often observed, indicating a high degree of dispersion due to sonication treatment.

To describe the diameter and length distribution of the MWNTs, random sampling of the tubes was used to obtain statistically significant and unbiased results. Diameter was measured (using iTEM software) from edge to edge and at the widest part of a MWNT, while length was measured along the curved contour of the tube. Figure 3a shows the diameter distribution of sonicated MWNTs, with each bar representing a diameter range of 1 nm. The percent-average diameter of the sonicated MWNTs is  $17.6 \pm 7.9$  nm, which is slightly higher than the unsonicated MWNTs ( $15.3 \pm 7.4$  nm, SI Figure S2a). Figure 3b shows the length distribution of the sonicated MWNTs, with each bar representing a length range of 0.25  $\mu\text{m}$ . This result confirms the TEM observation (Figure 2b) of significant shortening of MWNTs due to successive sonication. The sonicated MWNTs had a percent-average length of  $1.5 \pm 1.5 \mu\text{m}$ , much shorter than the unsonicated MWNTs ( $6.6 \pm 6.8 \mu\text{m}$ , SI Figure S2b).

**MWNT Defects and Impurities.** A typical Raman spectrum (SI Figure S3) exhibits three main bands: near  $200 \text{ cm}^{-1}$ , called radial breathing mode (RBM), due to in-phase atomic vibration on radial direction; near  $1600 \text{ cm}^{-1}$ , called the G-band, due to in-plane bond-stretching; and near  $1350 \text{ cm}^{-1}$ , called the D-band, due to weak disorder or defects (30–32). The first-order Raman spectra in SI Figure S3 showed prominent G and D bands. The RBM for MWNTs showed a weak signature which is characteristic of multiple-concentric walled CNTs and is consistent with other findings (33). The Raman spectra were taken using both 785 and 532 nm lasers. The defect band is usually more pronounced for the 785 nm laser excitation (34). Using this laser, the estimated G/D ratio of the MWNTs after sonication decreased from 0.24 to 0.18, indicating the presence of a higher degree of defects for sonicated MWNTs.

TGA data for unsonicated MWNTs are presented in SI Figure S4. The mass loss profile in SI Figure S4a shows that the major onset of oxidation of MWNTs occurred  $\sim 400$  °C. The plateau beyond 630 °C resulted in residual mass of 8.3% of the total mass of the sample, which can be attributed to the catalyst metal oxide content of the MWNT sample. The derivative of mass loss profile (SI Figure S4b) shows the major peak, i.e., the maximum rate of oxidation, occurring at 580 °C, which is characteristic of MWNT oxidation (35), with a smaller peak ( $<1\%$  of the total mass) at  $\sim 300$  °C, indicative of the presence of amorphous carbon.

**Aggregation Kinetics in the Presence of Monovalent ( $\text{Na}^+$ ) Cations.** The attachment efficiency,  $\alpha$ , of MWNTs as a function of monovalent ( $\text{Na}^+$ ) cations (1–500 mM) at unadjusted pH ( $\text{pH } 6.0 \pm 0.2$ ) is presented in Figure 4. At pH 6.0 the MWNTs are negatively charged, thereby exhibiting strong electrostatic repulsion at low ionic strengths. Distinct unfavorable (slow) and favorable (fast) aggregation kinetics regimes, demarcated by the critical coagulation concentration (CCC), are observed, indicating electrostatic, Derjaguin–Landau–Verwey–Overbeek (DLVO) type interactions to be the dominant mechanism for stabilization (23, 24). At low ionic strength conditions, an increase in salt concentration leads to a corresponding increase in attachment efficiency. This

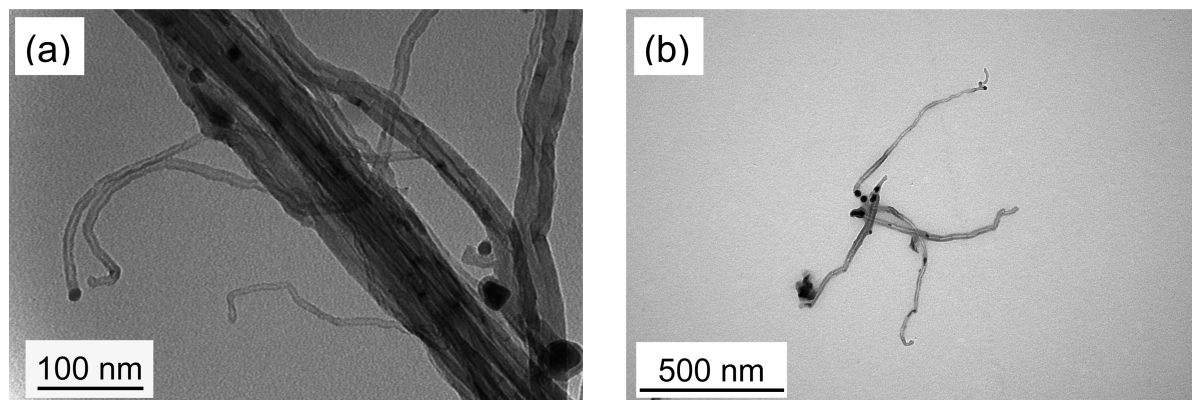


FIGURE 2. TEM images of representative MWNTs (a) before and (b) after sonication treatment (six cycles). Highly bundled, untreated MWNTs (on left) debundle and become shorter after successive sonication (on right).

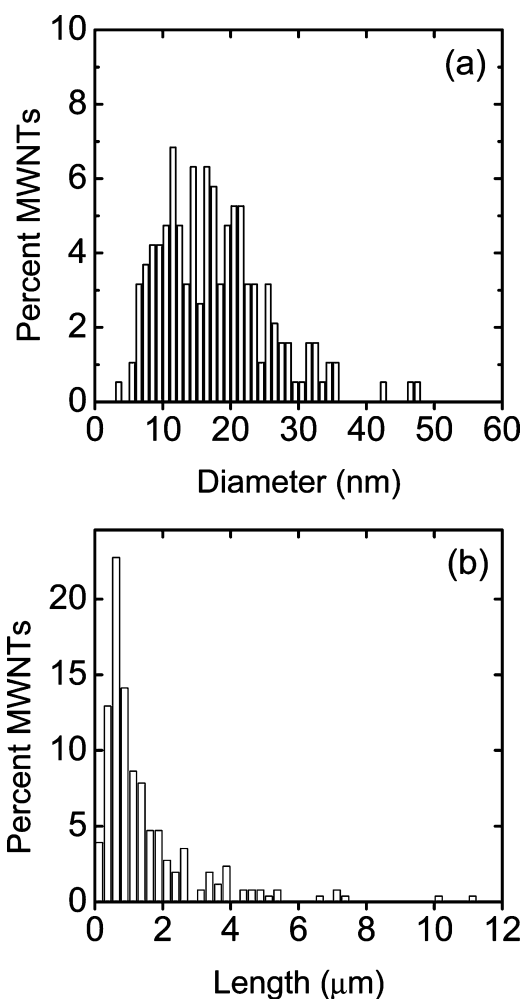


FIGURE 3. MWNT (a) diameter distribution and (b) length distribution after treatment as obtained from TEM imaging. More than 100 tubes were measured for each plot to obtain the distribution. The average diameter after treatment was measured as  $17.6 \pm 7.9$  nm and the average length was measured as  $1.5 \pm 1.5$   $\mu$ m.

is consistent with the EPM behavior (Figure 1a), where an increase in NaCl concentration leads to less negative MWNT EPM values. At higher ionic strength conditions, an increase in salt concentration has no effect on attachment efficiency. Under these conditions, the electrostatic repulsion between MWNTs is completely suppressed and every collision between MWNTs results in attachment. The critical coagulation concentration (CCC), obtained from the intersection of the

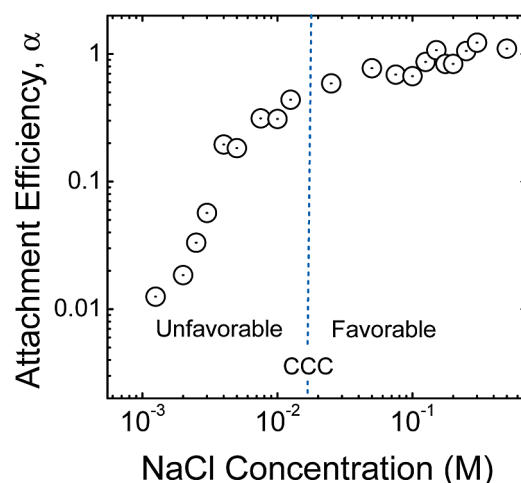
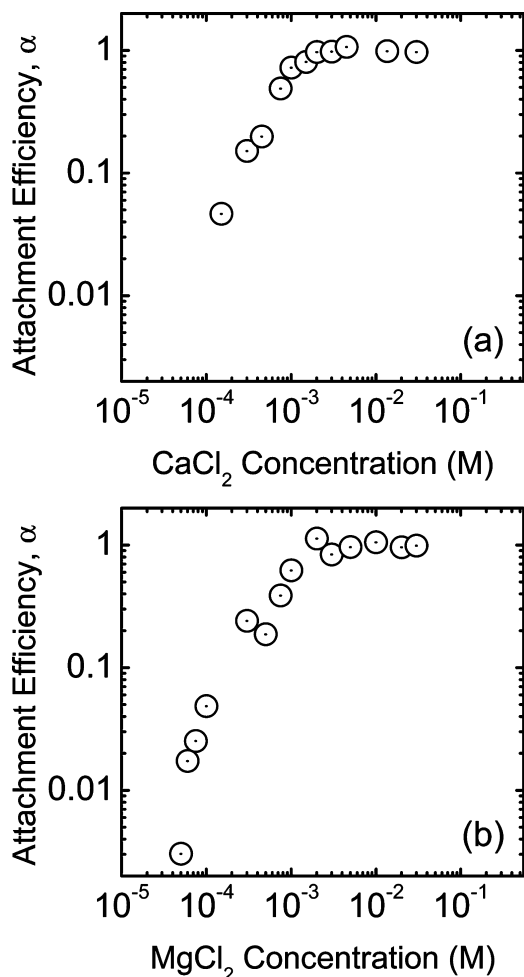


FIGURE 4. Attachment efficiencies of MWNTs as a function of NaCl concentration at unadjusted pH ( $\text{pH } 6.0 \pm 0.2$ ). The critical coagulation concentration (CCC) is based on the intersection of the extrapolations of the unfavorable and favorable regimes and estimated as 25 mM NaCl. Aggregation experiments are carried out at room temperature ( $23^\circ\text{C}$ ).

interpolated lines through the unfavorable and favorable regimes, is 25 mM NaCl. Our derived CCC value for MWNTs is close to a previously reported CCC value for SWNTs (37 mM NaCl), obtained from turbidity experiments (12). Note that reported CCC values for other carbon-based nanomaterials, specifically fullerene nanoparticles, are much higher: 85 mM, 160 mM, and 120 mM NaCl (21, 24).

**Aggregation Kinetics in the Presence of  $\text{Ca}^{2+}$  and  $\text{Mg}^{2+}$  Cations.** The aggregation kinetics of MWNTs were also examined for divalent cations:  $\text{Ca}^{2+}$  (0.1–30 mM) and  $\text{Mg}^{2+}$  (0.05–30 mM). Figure 5 shows the attachment efficiencies of MWNTs as a function of  $\text{Ca}^{2+}$  (Figure 5a) and  $\text{Mg}^{2+}$  (Figure 5b), revealing similar DLVO type behavior to that of NaCl, with distinct unfavorable and favorable aggregation kinetics regimes. The CCC values obtained are 2.6 mM  $\text{CaCl}_2$  and 1.5 mM  $\text{MgCl}_2$ , which are an order of magnitude lower than that of NaCl. Previously reported CCC values for SWNTs were 0.2 mM  $\text{CaCl}_2$  and 0.3 mM  $\text{MgCl}_2$ , respectively (12), significantly lower than our observed values. Higher CCC values were reported for fullerenes, namely 4.1–6.0 mM  $\text{CaCl}_2$  and 8.0 mM  $\text{MgCl}_2$  (21, 24, 36). The observed weak dependence of the MWNT CCC values on counterion valence is consistent with observations with colloidal particles (37), where CCC dependence on counterion valence  $z$  ranges from  $z^{-2}$  to  $z^{-6}$  (Schulze-Hardy Rule). The higher aggregation rate of MWNTs in the presence of divalent cations is consistent with the



**FIGURE 5.** Attachment efficiencies of MWNTs as a function of (a)  $\text{CaCl}_2$  and (b)  $\text{MgCl}_2$  concentrations at unadjusted pH ( $\text{pH } 6.0 \pm 0.2$ ). The critical coagulation concentration (CCC) values are based on the intersection of the extrapolations of the unfavorable and favorable regimes, and estimated as 2.6 mM  $\text{CaCl}_2$  and 1.5 mM  $\text{MgCl}_2$ . Aggregation experiments are carried out at room temperature ( $23^\circ\text{C}$ ).

EPM behavior in Figure 1a, where the EPM values become much less negative with divalent salts.

**Effect of pH on MWNT Aggregation Kinetics.** The stability of MWNTs in aqueous solution exhibited a strong pH dependence (Figure 6). As pH is increased from acidic (pH 3) to strong basic (pH 11) conditions, the attachment efficiency decreased sharply from a value of  $0.3 (\pm 0.05)$  to  $0.002 (\pm 0.001)$ . This behavior is indicative of dissociation of functional groups in changing pH conditions. As discussed earlier, functional groups can form on CNT surfaces by imparting mechanical energy to the system (38). Extensive high power sonication of MWNTs can result in defects and addition of functional groups. The slow aggregation rate of MWNTs at high pH (SI Figure S5) can therefore be explained by dissociation of functional groups on the MWNT surface. This observation is supported by the EPM data presented earlier (Figure 1b) where a more negative charge (or EPM) is observed as the pH is increased from acidic to basic conditions.

#### Humic Acid Significantly Enhances MWNT Stability.

Figure 7 shows a significant decrease in attachment efficiencies in the presence of SRHA for aqueous solutions containing monovalent and divalent salts. Previous studies attributed the association of humic and fulvic acid molecules with fullerenes and MWNTs to  $\pi$ - $\pi$  interactions between the cross-linked aromatic networks on the molecules and the

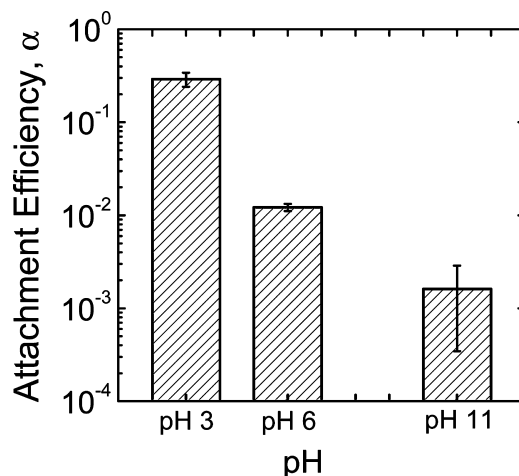


**FIGURE 6.** Attachment efficiencies of MWNTs as a function of solution pH in the presence of 1 mM background NaCl. The attachment efficiencies are calculated by normalizing the actual aggregation rate to the favorable (fast) aggregation rate with NaCl (raw data of Figure 4). Aggregation experiments were carried out at room temperature ( $23^\circ\text{C}$ ).

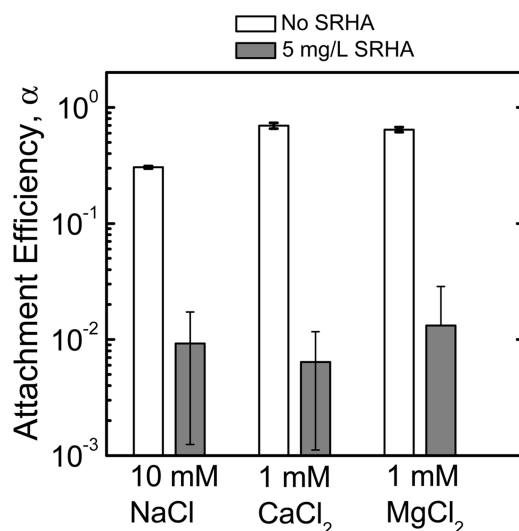


**FIGURE 7.** Attachment efficiencies in the absence and presence of 5 mg/L Suwannee River humic acid (SRHA) for different electrolyte solutions. pH for the SRHA was preadjusted to 6.0. The attachment efficiencies are calculated by normalizing the actual aggregation rate with the favorable aggregation rate of NaCl,  $\text{CaCl}_2$ , and  $\text{MgCl}_2$ , respectively (raw data of Figure 4 and Figure 5). The aggregation experiments were performed at room temperature  $23^\circ\text{C}$ . Solution pH for runs without SRHA was unadjusted ( $6.0 \pm 0.2$ ).

aromatic rings on the fullerenes (39–41). Enhanced stability of fullerenes in the presence of humic acid (21, 41, 42), fulvic acid (41, 42), and human serum albumin (43), has been well established in the literature. The dramatic decrease in MWNT aggregation kinetics (SI Figure S6), with 1–2 orders of magnitude reduction in attachment efficiencies, is attributed to non-DLVO, steric interactions imparted by the adsorbed humic macromolecules. EPM values in the presence of SRHA remained unchanged (SI Figure S1), indicating that the enhanced stability cannot be due to higher electrostatic repulsion. Steric stabilization by natural organic matter has been observed for fullerene nanoparticles, clay, iron oxide nanoparticles, and aquatic colloids (21, 44–46).

**Implications for Fate and Transport in Aquatic Environments.** Typical aquatic environments—rivers, lakes, estuaries, and groundwater—contain monovalent and di-

valent salts as well as natural organic matter. The fundamental understanding of the aggregation behavior of nanomaterials at these solution chemistries is the key to predicting their transport and fate in aquatic environments. Results with our MWNT sample suggest that MWNTs can be relatively stable under solution chemistries typical of aquatic environments. The aggregation of MWNTs followed DLVO type behavior that is in principle similar to that of most other aqueous colloidal particles. However, the results may not be generalized for all commercial MWNTs as there might be differences in physicochemical properties between samples, depending on synthesis and treatment methods. Suspended particles and colloidal matter are abundant in aquatic environments, suggesting that MWNT–MWNT interactions may not be the dominant process controlling the fate and transport of these nanomaterials. MWNTs will most likely interact more with suspended and colloidal particles. Therefore, further studies on aggregation behavior of MWNTs in the presence of environmentally relevant particles is of great importance.

### Acknowledgments

Funding was provided by the National Science Foundation (BES 0646247). We are grateful to the late Dr. Marc Pypaert (Department of Cell Biology, Yale University School of Medicine) for taking the TEM images used in this study. We also express our gratitude to Dr. Kai Loon Chen and Codruta Zoican (Department of Chemical Engineering, Yale University) for assistance in DLS and Raman spectroscopy measurements, respectively.

### Supporting Information Available

The electrophoretic mobilities of MWNTs in the presence and absence of SRHA for 10 mM NaCl, 1 mM CaCl<sub>2</sub>, and 1 mM MgCl<sub>2</sub> solution conditions are presented in Figure S1. The diameter and length distribution of the MWNTs before sonication treatment are presented in Figure S2. In Figure S3, Raman spectra of MWNTs before and after sonication are presented for both 785 and 532 nm lasers. TGA mass loss and mass loss derivative profiles are presented in Figure S4. Representative aggregation profiles of MWNTs as a function of pH are presented in Figure S5. In Figure S6, representative aggregation profiles of MWNTs in the presence and absence of SRHA are presented. This material is available free of charge via the Internet at <http://pubs.acs.org>.

### Literature Cited

- Liu, J.; Rinzler, A. G.; Dai, H. J.; Hafner, J. H.; Bradley, R. K.; Boul, P. J.; Lu, A.; Iverson, T.; Shelimov, K.; Huffman, C. B.; Rodriguez-Macias, F.; Shon, Y. S.; Lee, T. R.; Colbert, D. T.; Smalley, R. E. Fullerene pipes. *Science* **1998**, *280*, 1253–1256.
- Mauter, M. S.; Elimelech, M. Environmental applications of carbon-based nanomaterials. *Environ. Sci. Technol.* **2008**, *42*, 5843–5859.
- Iijima, S.; Ichihashi, T. Single-shell carbon nanotubes of 1-nm diameter. *Nature* **1993**, *363*, 603–605.
- Iijima, S. Helical microtubules of graphitic carbon. *Nature* **1991**, *354*, 56–58.
- Rosen, R.; Simendinger, W.; Debbault, C.; Shimoda, H.; Fleming, L.; Stoner, B.; Zhou, O. Application of carbon nanotubes as electrodes in gas discharge tubes. *Appl. Phys. Lett.* **2000**, *76*, 1668–1670.
- Che, G. L.; Lakshmi, B. B.; Fisher, E. R.; Martin, C. R. Carbon nanotubule membranes for electrochemical energy storage and production. *Nature* **1998**, *393*, 346–349.
- Ajayan, P. M.; Stephan, O.; Colliex, C.; Trauth, D. Aligned carbon nanotube arrays formed by cutting a polymer resin-nanotube composite. *Science* **1994**, *265*, 1212–1214.
- Baughman, R. H.; Cui, C.; Zakhidov, A. A.; Iqbal, Z.; Barisci, J. N.; Spinks, G. M.; Wallace, G. G.; Mazzoldi, A.; De Rossi, D.; Rinzler, A. G.; Jaszinski, O.; Roth, S.; Kertesz, M. Carbon nanotube actuators. *Science* **1999**, *284*, 1340–1344.

- Wu, W.; Wieckowski, S.; Pastorin, G.; Benincasa, M.; Klumpp, C.; Briand, J. P.; Gennaro, R.; Prato, M.; Bianco, A. Targeted delivery of amphotericin B to cells by using functionalized carbon nanotubes. *Angew. Chem.-Int. Ed.* **2005**, *44*, 6358–6362.
- Wiesner, M. R.; Lowry, G. V.; Alvarez, P.; Dionysiou, D.; Biswas, P. Assessing the risks of manufactured nanomaterials. *Environ. Sci. Technol.* **2006**, *40*, 4336–4345.
- Thess, A.; Lee, R.; Nikolaev, P.; Dai, H. J.; Petit, P.; Robert, J.; Xu, C. H.; Lee, Y. H.; Kim, S. G.; Rinzler, A. G.; Colbert, D. T.; Scuseria, G. E.; Tomanek, D.; Fischer, J. E.; Smalley, R. E. Crystalline ropes of metallic carbon nanotubes. *Science* **1996**, *273*, 483–487.
- Sano, M.; Okamura, J.; Shinkai, S. Colloidal nature of single-walled carbon nanotubes in electrolyte solution: The Schulze-Hardy rule. *Langmuir* **2001**, *17*, 7172–7173.
- Jiang, L. Q.; Gao, L.; Sun, J. Production of aqueous colloidal dispersions of carbon nanotubes. *J. Colloid Interface Sci.* **2003**, *260*, 89–94.
- Lisunova, M. O.; Lebovka, N. I.; Melezhyk, E. V.; Boiko, Y. P. Stability of the aqueous suspensions of nanotubes in the presence of nonionic surfactant. *J. Colloid Interface Sci.* **2006**, *299*, 740–746.
- Jung, D. H.; Ko, Y. K.; Jung, H. T. Aggregation behavior of chemically attached poly(ethylene glycol) to single-walled carbon nanotubes (SWNTs) ropes. *Mater. Sci. Eng., C* **2004**, *24*, 117–121.
- Chen, J.; Hamon, M. A.; Hu, H.; Chen, Y. S.; Rao, A. M.; Eklund, P. C.; Haddon, R. C. Solution properties of single-walled carbon nanotubes. *Science* **1998**, *282*, 95–98.
- Chen, Q.; Saltiel, C.; Manickavasagam, S.; Schadler, L. S.; Siegel, R. W.; Yang, H. C. Aggregation behavior of single-walled carbon nanotubes in dilute aqueous suspension. *J. Colloid Interface Sci.* **2004**, *280*, 91–97.
- Niyogi, S.; Boukhalfa, S.; Chikkannanavar, S. B.; McDonald, T. J.; Heben, M. J.; Doorn, S. K. Selective aggregation of single-walled carbon nanotubes via salt addition. *J. Am. Chem. Soc.* **2007**, *129*, 1898–1899.
- Phenrat, T.; Saleh, N.; Sirk, K.; Tilton, R. D.; Lowry, G. V. Aggregation and sedimentation of aqueous nanoscale zerovalent iron dispersions. *Environ. Sci. Technol.* **2007**, *41*, 284–290.
- Ertel, J. R.; Hedges, J. I.; Devol, A. H.; Richey, J. E.; Ribeiro, M. d. N. G. Dissolved humic substances of the Amazon river system. *Limnol. Oceanogr.* **1986**, *31*, 739–754.
- Chen, K. L.; Elimelech, M. Influence of humic acid on the aggregation kinetics of fullerene (C-60) nanoparticles in monovalent and divalent electrolyte solutions. *J. Colloid Interface Sci.* **2007**, *309*, 126–134.
- Hong, S. K.; Elimelech, M. Chemical and physical aspects of natural organic matter (NOM) fouling of nanofiltration membranes. *J. Membr. Sci.* **1997**, *132*, 159–181.
- Chen, K. L.; Elimelech, M. Aggregation and deposition kinetics of fullerene (C-60) nanoparticles. *Langmuir* **2006**, *22*, 10994–11001.
- Chen, K. L.; Mylon, S. E.; Elimelech, M. Aggregation kinetics of alginate-coated hematite nanoparticles in monovalent and divalent electrolytes. *Environ. Sci. Technol.* **2006**, *40*, 1516–1523.
- Clougherty, D. P.; Zhu, X. Stability and Teller's theorem: Fullerenes in the March model. *Phys. Rev. A* **1997**, *56*, 632–635.
- Leys, F. E.; Amovilli, C.; Howard, I. A.; March, N. H.; Rubio, A. Surface charge model of a carbon nanotube: self-consistent field from Thomas-Fermi theory. *J. Phys. Chem. Solids* **2003**, *64*, 1285–1288.
- Hirsch, A.; Vostrowsky, O. In *Functional Organic Materials: Syntheses, Strategies and Applications*; Müller, T. J. J., Bunz, U. H. F., Eds.; Wiley-VCH: Weinheim, 2005; pp 193–237.
- Li, Q. L.; Elimelech, M. Organic fouling and chemical cleaning of nanofiltration membranes: Measurements and mechanisms. *Environ. Sci. Technol.* **2004**, *38*, 4683–4693.
- Kamalakar, G.; Hwang, D. W.; Hwang, L. P. Synthesis and characterization of multiwalled carbon nanotubes produced using zeolite Co-beta. *J. Mater. Chem.* **2002**, *12*, 1819–1823.
- Popov, V. N. Carbon nanotubes: properties and application. *Mater. Sci. Eng. R* **2004**, *43*, 61–102.
- Saito, R.; Dresselhaus, G.; Dresselhaus, M. S. *Properties of Carbon Nanotubes*; Imperial College Press: London, 2005.
- Thomsen, C.; Reich, S.; Maultzsch, J. Resonant Raman spectroscopy of nanotubes. *Philos. Trans. R. Soc. London, Ser. A* **2004**, *362*, 2337–2359.
- Jantoljak, H.; Salvétat, J. P.; Forro, L.; Thomsen, C. Low-energy Raman-active phonons of multiwalled carbon nanotubes. *Appl. Phys. A: Mater. Sci. Process.* **1998**, *67*, 113–116.

- (34) Rao, A. M.; Bandow, S.; Richter, E.; Eklund, P. C. Raman spectroscopy of pristine and doped single wall carbon nanotubes. *Thin Solid Films* **1998**, *331*, 141–147.
- (35) Murphy, R.; Coleman, J. N.; Cadek, M.; McCarthy, B.; Bent, M.; Drury, A.; Barklie, R. C.; Blau, W. J. High-yield, nondestructive purification and quantification method for multiwalled carbon nanotubes. *J. Phys. Chem. B* **2002**, *106*, 3087–3091.
- (36) Mchedlov-Petrosyan, N. O.; Klochkov, V. K.; Andrievsky, G. V. Colloidal dispersions of fullerene C60 in water: some properties and regularities of coagulation by electrolytes. *J. Chem. Soc., Faraday Trans.* **1997**, *93*, 4343–4346.
- (37) Elimelech, M.; Gregory, J.; Jia, X.; Williams, R. A. *Particle Deposition and Aggregation: Measurement, Modelling and Simulation*; Williams, R. A., Ed.; Butterworth Heinemann: Oxford, England, 1995.
- (38) Pan, H. L.; Liu, L. Q.; Guo, Z. X.; Dai, L. M.; Zhang, F. S.; Zhu, D. B.; Czerw, R.; Carroll, D. L. Carbon nanotubols from mechanochemical reaction. *Nano Lett.* **2003**, *3*, 29–32.
- (39) Hyung, H.; Fortner, J. D.; Hughes, J. B.; Kim, J. H. Natural organic matter stabilizes carbon nanotubes in the aqueous phase. *Environ. Sci. Technol.* **2007**, *41*, 179–184.
- (40) Hyung, H.; Kim, J. H. Natural organic matter (NOM) adsorption to multi-walled carbon nanotubes: Effect of NOM characteristics and water quality parameters. *Environ. Sci. Technol.* **2008**, *42*, 4416–4421.
- (41) Terashima, M.; Nagao, S. Solubilization of [60] fullerene in water by aquatic humic substances. *Chem. Lett.* **2007**, *36*, 302–303.
- (42) Xie, B.; Xu, Z. H.; Guo, W. H.; Li, Q. L. Impact of natural organic matter on the physicochemical properties of aqueous C-60 nanoparticles. *Environ. Sci. Technol.* **2008**, *42*, 2853–2859.
- (43) Deguchi, S.; Yamazaki, T.; Mukai, S.; Usami, R.; Horikoshi, K. Stabilization of C-60 nanoparticles by protein adsorption and its implications for toxicity studies. *Chem. Res. Toxicol.* **2007**, *20*, 854–858.
- (44) Buffle, J.; Wilkinson, K. J.; Stoll, S.; Filella, M.; Zhang, J. W. A generalized description of aquatic colloidal interactions: The three-colloidal component approach. *Environ. Sci. Technol.* **1998**, *32*, 2887–2899.
- (45) Heidmann, I.; Christl, I.; Kretzschmar, R. Aggregation kinetics of kaolinite-fulvic acid colloids as affected by the sorption of Cu and Pb. *Environ. Sci. Technol.* **2005**, *39*, 807–813.
- (46) Tipping, E.; Ohnstad, M. Colloid stability of iron-oxide particles from a fresh-water lake. *Nature* **1984**, *308*, 266–268.

ES801251C